New observations of the distribution, morphology, and dissolution dynamics of cryogenic gypsum in the Arctic Ocean

Jutta E. Wollenburg[1*], Morten Iversen[1,2], Christian Katlein[1], Thomas Krumpen[1], Marcel Nicolaus[1], Giulia Castellani[1], Ilka Peeken[1], Hauke Flores[1]

[1]Alfred-Wegener-Institut Helmholtz-Zentrum für Polar- und Meeresforschung, D-27570, Bremerhaven, Germany

[2]MARUM and University of Bremen, D-27359, Bremen, Germany

[*]Corresponding author and requests for materials should be addressed to J.E.W. (email: Jutta.Wollenburg@awi.de)

Abstract

To date observations on a single location indicate that cryogenic gypsum ($Ca[SO_4]\cdot 2H_2O$) may constitute an efficient but hitherto overlooked ballasting mineral enhancing the efficiency of the biological carbon pump in the Arctic Ocean. In June-July 2017 we sampled cryogenic gypsum under pack-ice in the Nansen Basin north of Svalbard using a plankton net mounted on a Remotely Operated Vehicle (ROVnet). Cryogenic gypsum crystals were present at all sampled stations, which suggested a persisting cryogenic gypsum release from melting sea ice throughout the investigated area. This was supported by a sea-ice backtracking model indicating that gypsum release was not related to a specific region of sea ice formation. The observed cryogenic gypsum crystals exhibited a large variability in morphology and size, with the largest crystals exceeding a length of 1 cm. Preservation, temperature and pressure laboratory studies revealed that gypsum dissolution rates accelerated with increasing temperature and pressure, ranging from 6% d^{-1} by mass in Polar Surface Water (-0.5 °C) to 81% d^{-1} by mass in Atlantic Water (2.5 °C at 65 bar). When testing the preservation of gypsum in Formaldehyde-fixed samples we observed immediate dissolution. Dissolution at warmer temperatures and through inappropriate preservation media may thus explain why cryogenic gypsum was not observed in scientific samples previously. Direct measurements of gypsum crystal sinking velocities ranged between 200 and 7000 m d^{-1}, suggesting that gypsum-loaded marine aggregates could rapidly sink from the surface to abyssal depths, supporting the hypothesised potential of gypsum as a ballasting mineral in the Arctic Ocean.

Keywords:

Cryogenic gypsum, Arctic Ocean, mineral ballasting, biological carbon pump, sea ice.

Gelöscht:

Gelöscht: that indicated

Gelöscht: indicated

Gelöscht: .

1 Introduction

Climate change in the Arctic Ocean has led to a drastic reduction of summer sea ice extent as well as to a significant thinning of the sea ice (Kwok, 2018; Kwok and Rothrock, 2009). Sea ice strength has reduced, and increased deformation and fractionation result in a progressively increasing sea ice drift speed (Docquier et al., 2017) and sea-ice export. Over the past decades the ice export via the Fram Strait alone has increased by 11% per decade during the productive spring and summer period (Smedsrud et al., 2017). An increasing amount of sea ice produced in the East Siberian and Laptev Sea melts over the adjacent continental slopes or in the central Arctic Ocean (Krumpen et al., 2019). Overall, the Arctic Ocean sea ice cover has shifted to a predominantly seasonal ice cover. However, although the majority of sea ice diminishes during late summer, the amount of sea ice produced in autumn to winter progressively increases (Kwok, 2018).

Large-scale transformations in the seasonal sea-ice cover impact the physical, chemical and biological dynamics of the sea ice-ocean system. However, especially the interactions of physical-chemical processes within the sea ice and pelagic to benthic biological processes have only received little attention. Of particular importance are poorly soluble minerals precipitated within the brine channels of sea ice which, once released, may ballast organic material sinking to the sea-floor. The changing icescape with more leads and the thinner Arctic sea ice allows increasing light penetration into the under-ice surface water (Katlein et al., 2015; Nicolaus et al., 2013; Nicolaus et al., 2012), supporting fast-growing and often massive under-ice phytoplankton blooms (Arrigo et al., 2012; Arrigo et al., 2014; Assmy et al., 2017). A recent study reported on a sudden export event of an under-ice bloom of the 'unsinkable alga' *Phaeocystis*, caused by the ballasting effect of cryogenic gypsum released from melting sea ice (Wollenburg et al., 2018a). This single event was the first and only report of cryogenic gypsum release in the Arctic Ocean. Moreover, this sea ice precipitation of cryogenic gypsum has never been recorded in Arctic sediments, sediment traps or other field studies.

When sea ice forms, the concentrations of dissolved ions in brine increase, and depending on the temperature of sea ice, a series of minerals (ikaite, mirabilite, hydrohalite, gypsum, hydrohalite, sylvite, $MgCl_2$, Antarcticite) precipitate (Butler, 2016; Butler and Kennedy, 2015; Geilfus et al., 2013; Golden et al., 1998; Wollenburg et al., 2018a). Once released into the ocean, gypsum is considered to be the most stable of the cryogenic precipitates (Butler et al.,

Gelöscht:

Gelöscht: 6% and

Gelöscht: as annual mean, and

Gelöscht: , respectively

Gelöscht:

Gelöscht: seems

2017; Strunz and Nickel, 2001). Sea ice-derived cryogenic gypsum was first described by Geilfus et al. (Geilfus et al., 2013), in a comprehensive work on the chemical, physical, and mineralogical aspects of its precipitation in experimental and natural sea ice off Greenland. According to FREZCHEM, a chemical–thermodynamic model that was developed to quantify aqueous electrolyte properties at sub-zero temperatures, cryogenic gypsum can precipitate at temperatures below –18 °C, and within a small temperature window between –6.5 and –8.5 °C (Geilfus et al., 2013; Marion et al., 2010; Wollenburg et al., 2018a). However, measurements on the stoichiometric solubility products showed that gypsum dynamics in ice–brine equilibrium systems strongly depend on the solubility and precipitation of hydrohalite and mirabilite (Butler, 2016; Butler et al., 2017). So far gypsum precipitation in experimental setups were only observed at temperatures between -7.1 and -8.2 °C, and not in the lower temperature range (Butler, 2016; Butler et al., 2017). Moreover, as Arctic sea ice rarely reaches temperatures lower than -18 °C, cryogenic gypsum is more likely precipitated within the higher temperature window in the Arctic Ocean (Wollenburg et al., 2018a).

A model applied to understand the gypsum release event of 2015 showed that the ice floe was too warm when it started to form and identified December to February as the most likely time span for gypsum precipitation (Wollenburg et al., 2018a). Due to the absence of a downward brine flux in this advanced phase of sea ice formation, gypsum crystals likely remain trapped in the ice until spring. In the absence of sufficient field observations gypsum release from sea ice is expected to peak at the beginning of the melting season, when sea ice warms to temperatures above -5 °C. This temperature marks the transition in the fluid transport capacities of sea ice allowing brine water and included crystals to be released into the water column (Golden et al., 1998). However, in lack of any extensive year-round field studies our knowledge depends on models, kinetics and two single field observations (Geilfus et al., 2013; Wollenburg et al., 2018a). There are no studies on sea ice-derived cryogenic gypsum crystal morphologies and its stability in seawater. It is unclear whether gypsum just precipitates during the assumed peak in December to February or whether it continues to grow in remaining brines during sea ice drift.

In this study, we systematically investigated the occurrence of cryogenic gypsum release from sea ice in spring 2017 with special emphasis on the morphological properties of the crystals. Varieties of cryogenic gypsum crystal morphologies are described and illustrated. The sampled gypsum crystals were further subjected to various laboratory experiments. Hereby, we investigated the dissolution behaviour over typical depth- and temperature ranges of the

Gelöscht:

Gelöscht: firstly

Gelöscht: flow

Gelöscht: to

Gelöscht: best

Gelöscht: from

Gelöscht: We therefore need more studies on the formation and release of cryogenic gypsum to assess its impact on biogeochemistry in the Arctic and sub-Arctic.

Gelöscht: overall appearance

Arctic water column and in Formaldehyde solution typically used for biological sampling preservation. We also made direct measurements of the size-specific sinking speed of individual gypsum crystals. These experiments were conducted to answer the question, why cryogenic gypsum has not previously been observed in field studies and if it qualifies as ballast mineral.

Gelöscht: ,
Gelöscht: in
Gelöscht: were investigated and
Gelöscht: crystal measured.

2 Material and Methods

2.1 Gypsum sampling with the ROVnet and on-board treatment

RV *Polarstern* expedition PS 106 (June-July 2017) in the early melting season gave the opportunity to systematically study the occurrence of cryogenic gypsum release and the morphological properties of gypsum crystals in the area north of Svalbard and on the Barents Sea shelf (Fig. 1A; Table 1).

Gelöscht: overall appearance
Gelöscht: the

Cryogenic gypsum was sampled from the upper 10 m of the under-ice water at four stations distributed throughout the expedition area (Fig. 1A; Table 1). The first part of the expedition (PS106/1) consisted of a drift study to the north of Svalbard, during which the vessel was anchored to an ice floe (station 32). This ice floe was revisited 6 weeks later at the end of the expedition (PS106/2) (station 80). During the second part of the expedition (PS106/2), cryogenic gypsum was collected over the western Barents Sea (station 45) and in the Nansen Basin to the north-east of Svalbard (station 66).

Gypsum crystals were sampled with a plankton net mounted on a remotely operated vehicle (ROVnet, Fig. S1). The ROVnet consists of a Polycarbonate frame with an opening of 40 cm by 60 cm, to which a zooplankton net with a mesh size of 500 μm was attached (Flores, 2018). For gypsum sampling, a handmade nylon net with an opening of 10 cm by 15 cm and a mesh size of 30 μm was mounted in the zooplankton net opening. The concentrated particulate material of the small nylon net was collected in a 2 L polyethylene bottle attached to the cod end of the net. A gauze-covered window in the cod-end bottle allowed seawater to drain off. Both nets were mounted on the aft end of a M500 (Ocean Modules, Sweden) observation class ROV carrying an extensive sensor suite described in Katlein et al. (Katlein

et al., 2017). After each ROVnet deployment, the nets were rinsed with ambient sea-water to concentrate the sample in the cod end of the net. The ROVnet sampled horizontal profiles in the water directly below the sea ice. Standard ROVnet profiles were conducted at the ice-water interface, at 5 m and at 10 m depth. The distance covered by each profile ranged between 300 and 600 m. At station 32, the 10 m profile was aborted due to technical failure, and at station 80 no 5 m profile was sampled due to time constraints, and the subsurface sample was discarded due to handling failure (Table 1).

The concentrated particulate material collected in the cod-end bottle of the gypsum sampling net was mixed with a sample equivalent volume of 98% ethanol, and stored at 4 °C until further analyses (Wollenburg et al., 2018a).

At ROVnet sampling stations, ice thickness was estimated through thickness drill holes with a tape measure. To characterize the properties of the ice floes sampled on the floe-wide scale, ice thickness surveys were conducted at each sampling station with a GEM2 (Geophex) electromagnetic induction ice-thickness sensor (Katlein et al., 2018).

2.2 Initial analyses of ROVnet samples

In the home laboratory the samples were rinsed onto a 32 μm mesh using fresh water. The samples were then oven-dried at 50°C for 20 hours. The remaining crystals were transferred into pre-weighed micropaleontological slides, and their weight was determined with a high-precision Sartorius SE2 ultra-microbalance. Under a Zeiss Axio Zoom V16 microscope, pictures were taken with an Axiocam 506 colour camera. We made both overview images of the whole sample and detailed images of individual crystals. From all samples and crystal morphologies, individual crystals were analysed using Raman microscopy, which confirmed that the crystals were gypsum (Wollenburg et al., 2018a). As in some samples both, very large and very small crystals (Figs. S3-S4) were observed, the >32 μm samples were dry-sieved over a 63 μm analysis sieve. The length and width of the cryogenic gypsum crystals in the size fractions >32<63 μm and >63 μm was determined with the software application ImageJ on 50 crystals in each sample and size fraction (Schneider et al., 2012) (Tab. 2).

2.3 Initial analyses of ice cores

At all ice stations, sea ice cores for archive purposes and for further measurement of bottom communities were drilled with a 9 cm diameter ice corer (Kovacs Enterprise) and stored at -

20°C (Peeken, 2018). One ice-core from station 80 and four bottom slices (10 cm) of ice-cores from station 45 were studied to investigate the gypsum crystal morphologies within sea ice. Each section was transferred into a measuring jug with lukewarm tap water for approx. two seconds, and then the jug was emptied over a 32 μm analysis sieve, and repeatedly refilled. This process was continued until all ice was melted. With the aid of a hand shower and a wash bottle the residue on the sieve was rinsed and transferred into a 30 μm mesh-covered funnel, dried and transferred into a micropaleontological picking tray for inspection and documentation. For storage, the residue was transferred into pre-weighed labelled micropaleontological slides.

2.4 Dissolution experiments

The aim of our dissolution experiments was to investigate the persistence of gypsum crystals against dissolution in the Arctic water column (water mass trials) and under common biological sample treatment (Formaldehyde trial).

Dissolution experiments were carried out on individual gypsum crystals collected from ROVnet samples. Hereby, 5 cryogenic gypsum crystals with different crystal morphologies, and from both size fractions were used in each reaction chamber. Before the start and after the termination of each experiment, pictures of the cryogenic gypsum crystals used were taken with an Axiocam 506 colour camera under a Zeiss Axio Zoom V16 microscope. The weight of the crystals before and after each treatment was determined with a high-precision Sartorius SE2 ultra-microbalance after they had been transferred into a pre-weighted silver boat. The experimental running time of each experiment was 24 hours.

2.4.1 Water mass trials

The experiments to simulate dissolution within the different water masses and hydrostatic pressure regimes of the Arctic Ocean were carried out with high-pressure chambers installed in a cooling table (Wollenburg et al., 2018b). With a high-pressure pump (ProStar218 Agilent Technologies), peak tubing, and multiple titanium valves a continuous isobaric and isocratic one-way seawater flow of 0.3 ml/min was directed through a set of four serially arranged high-pressure chambers each with an internal volume of 0.258 ml (Wollenburg et al., 2018b). This setup allowed for dissolution experiments at defined pressures and temperatures (Wollenburg et al., 2018b). For the experiments, we used sterile-filtered (0.2 µm mesh) North Sea water that was adjusted to a salinity of 34.98 by addition of 1 g Instant Ocean® sea salt

per L and psu-offset. The natural pH of 8.1 after equilibration to the refrigerator's atmosphere (at 2.5 °C and at atmospheric pressure), lowers to pH 8.05 at 2.5 °C at 150 bar (Culberson and Pytkowicx, 1968). Five experiments, with 4 high-pressure chambers were carried out. The Polar Surface (PSW) water corresponding experimental trial was running at -0.5 °C and 3 bar, the experimental Atlantic Water (AW) trial at +2.5 °C and 65 bar, and three experimental Deep Water trials were conducted at -1 °C and 100, 120 and 150 bar, respectively.

2.4.2 Formaldehyde trial

To study the effect of Formaldehyde treatment on cryogenic gypsum, the crystals were subjected to a Formaldehyde solution of 4% in seawater, which is commonly used to preserve biological samples. The stock solution consisted of 500 ml Formaldehyde concentration of 40%, 500 ml aqua dest. and 100 g hexamethylenetetramine, adjusted to a pH of 7.3-7.9. Aliquots of the 20% stock solution were added to the four-fold volume of artificial Arctic Ocean sea water to obtain a final concentration of 4%.

The Gypsum crystals were transferred into Falcon Tubes, and the 4% Formaldehyde solution was added. The Falcon tubes were then either stored at 3 °C, or at room temperature. After the experiments, the gypsum crystal-Formaldehyde suspension was washed with deionized water over a 10 μm mesh using a wash bottle, and dried on gauze. As in all formaldehyde trials all gypsum dissolved, no post-experimental weight was determined.

2.5 Size-specific settling velocities of gypsum

The size-specific sinking velocity of cryogenic gypsum was measured in a settling cylinder (Ploug et al., 2008). The cylinder (30 cm high and 5 cm in diameter) was filled with filtered seawater (salinity 32) and surrounded by a water jacket for thermal stabilization at 2 °C. The settling cylinder was closed at both ends, only allowing insertion of a wide-bore pipette at the top. Immediately before measurement, the gypsum was submerged into seawater with a salinity of 32 and a temperature of 2 °C, and then transferred to the settling cylinder with a wide-bore pipette. The gypsum crystals were allowed to sink out of the wide-bore pipette, which was centered in the cylinder. The descent of the crystals was recorded by a Basler 4 MPixel Ethernet camera equipped with a 25 mm fixed focal lens (Edmund Optics). The settling column was illuminated from the sides by a custom-made LED light source. The camera recorded 7 images per second as the gypsum crystals sank through the settling column. The setup was calibrated by recording a length scale before sinking velocity measurements. The size and settling of the individual gypsum crystals was determined with

Gelöscht: pellets

the image analysis software ImageJ. This was done by using the projected area of the crystals to calculate the equivalent spherical diameter and the distance traveled between the subsequent images to determine the sinking velocity of the individual crystals (Iversen et al., 2010)

We calculated the excess density ($\Delta\rho$) ($\Delta\rho$ = gypsum density – water density) of the crystal from the Stokes drag equation:

$$\Delta\rho = \frac{C_D \rho_w SV^2}{\frac{4}{3} gESD} \quad (1)$$

where C_D is the dimensionless drag force (equation 2), ρ_w is the density of seawater (1.0256 g cm^{-3}, for a salinity of 32 at 2 °C), SV is the measured sinking velocity in cm s^{-1}, g is the gravitational acceleration of 981 cm s^{-2}, and ESD is the equivalent spherical diameter in cm. We calculated C_D using the drag equation for low Reynolds numbers (White, 1974):

$$C_D = \left(\frac{24}{Re}\right) + \left(\frac{6}{1+Re^{0.5}}\right) + 0.4 \quad (2)$$

where the Reynolds number (Re) was defined as

$$Re = SV\ ESD\ \frac{\rho_w}{\eta} \quad (3)$$

where η is the dynamic viscosity (1.7545×10^{-2} g cm^{-1} s^{-1} for a salinity of 32 at 2 °C). Equation 2 is valid up to a Reynolds number of 2x10^5 (Vogel and Beety, 1994). The gypsum crystals had Reynolds numbers ranging from 0.77 to 128.

2.6 Backtracking the sampled ice flows under which cryogenic gypsum was sampled

To determine sea ice drift trajectories of sampled sea ice we used a Lagrangian approach (IceTrack) that traces sea ice backward or forward in time using a combination of satellite-derived low resolution drift products. So far, IceTrack has been used in a number of publications to examine sea ice sources, pathways, thickness changes and atmospheric processes acting on the ice cover (Damm et al., 2018{Peeken, 2018 #13678; Krumpen et al., 2016; Peeken et al., 2018). A detailed description is provided in Krumpen et al. (Krumpen et al., 2019).

Sea ice motion information was provided by different institutions, obtained from different sensors, and for different time intervals. In this study we applied a combination of three different products: (i) motion estimates based on a combination of scatterometer and radiometer data provided by the Center for Satellite Exploitation and Research (CERSAT (Girard-Ardhuin and Ezraty, 2012), (ii) the OSI-405-c motion product from the Ocean and Sea Ice Satellite Application Facility (OSISAF (Lavergne, 2016), and (iii) Polar Pathfinder Daily Motion Vectors from the National Snow and Ice Data Center (NSIDC (Tschudi et al., 2016).

The tracking approach works as follows: An ice parcel is traced backward or forward in time on a daily basis. Tracking is stopped if a) ice hits the coastline or fast ice edge, or b) ice concentration at a specific location drops below 50% and we assume the ice to be formed or melted. The applied sea ice concentration product was provided by CERSAT and was based on 85 GHz SSM/I brightness temperatures, using the ARTIST Sea Ice (ASI) algorithm.

3 Results

3.1 Presence and distribution of cryogenic gypsum under the investigated ice-floes

Based on backtracking (Krumpen, 2018) and sea ice observations, the sampled ice-floes had an age of 1 to 3 years (Fig. 1B) and were originating from the Siberian Sea (station 32/80), the Laptev Sea (station 45), and were more locally grown in the Nansen Basin (station 66). Whereas the mean sea ice thickness at the ROV survey stations ranged between 94 and 156 cm, the mean sea ice thickness of the investigated ice-floes estimated by an ice-thickness sensor surveys (Katlein et al., 2018) was 1.90 m for station 32, 1.00 m for station 45, and 1.80 m for stations 66 and 80 (Fig. 1A, Table 1). Despite the different origins and thicknesses of sea ice, cryogenic gypsum crystals were found at all stations and in all depth layers sampled with the ROVnet (Figs. 1A, B, Tab. 1). At all stations and sampling depths the samples were dominated by cryogenic gypsum, with a proportional dry weight of >96.5% in the 5 m-sample at station 32, and with >99% in all other samples (Figs. 2, Figs. S2-S5). Other lithogenic particles, as often found in sea ice (Nürnberg et al., 1994), were essentially absent.

Gelöscht: S1-S4

3.2 The morphology of cryogenic gypsum

The samples collected at station 32 were dominated by rounded, matte, solid cryogenic gypsum crystals with a mean length-width ratio of 1.40-1.76 (Tab. 2, S2). The proportional mass contribution of the smaller-sized crystals of the >30<63 μm size fraction increased with depth and outweighed the contribution of the >63 μm size fraction with 56.30%, and 66.28% for the 0 and 5 m water depth sample, respectively (Fig. 3). At 0 m, the mean length of the crystals was 68.46 μm in the >63 μm size fraction and 44.27 μm in the >30<63 μm fraction. At 5 m depth, crystal dimensions were similar, ranging at mean crystal lengths of 63.28 μm in the >63 μm, and 35.90 μm in the >30<63 μm size fraction, respectively.

At station 45, the crystals were mostly solid and for most part hyaline, rather than matte crystals as at station 32 (Figs. 2C-D, 6, S3). With decreasing weight proportion, the >63 μm size clearly dominated the 0, 5, and 10 m samples with 79.90, 73.39, and 66.14%, respectively. In the 0 m layer samples, mean crystal lengths were 114.18 μm in the >63 μm size fraction and 58.74 μm in the >30<63 μm size fraction (Tab. 2). At 5 m depth, we observed mean crystal lengths of 111 μm in the >63 μm size fractions, and 56.73 μm in the >30<63 μm fraction. The mean crystal lengths in the 10 m sample was 92.83 and 50.32 μm for the >63 and >30<63 μm size fraction, respectively. At station 45 the crystal length-width ratio varied between 1.37 and 1.98, measured in the >30<63 μm size fraction of the surface sample, and the >63 μm size fraction of the 10 m sample. The cryogenic gypsum crystals retrieved from the melted ice core drilled at this station were solid and hyaline. In size and shape they resembled the crystals of the 10 m layer at this station, with a mean crystal length of 114.2 μm, mean width of 57.2 μm, and a length-width ratio of 2 (Fig. 4).

At station 66, the crystals from 0 m water depth were dominated by large, pencil-like, hyaline and solid crystals with a mean crystal length of 1,355 μm and mean width of 415 μm in the dominating >63 μm fraction (99.25% mass) (Fig. 2B, S4, Tab. 2). These crystals with an average length-width ratio of 3.27 were found as isolated crystals, but very often also as inter-grown crystal rosettes with two to more than 10 individual crystals involved (Fig. S4; Tab. 2). The >30<63 μm size fraction (0.75% mass) was dominated by matte, whitish, rounded gypsum particles and tiny gypsum needles with a mean crystal length of 56.67 μm (Fig. S4, Tab. 2.). As at the other stations the weight proportion of the >63 μm size fraction significantly decreased from 99.25 in the 0 m, to 75.23 at 5 m, and 61.18% in the 10 m sample (Fig. 2). The size of cryogenic gypsum crystals collected from the 5 and 10 m layers was significantly smaller and predominantly composed of isolated small hyaline and euhedral gypsum needles. The length-width ratio ranged between 5.60 (5 m) and 4.37 (10 m) (Figs.

Gelöscht: S1

Gelöscht: S2

Gelöscht: S3

Gelöscht: S3

Gelöscht: S3

2A, S4, Tab. 2). In the 5 m layer sample, the mean crystal length was 411.42 μm in the >63 μm size fraction, and 62.03 μm in the >30<63 μm size fraction. The 10 m samples showed a mean crystal length of 101.40 μm in the >63, and 30.71 μm in the >30<63 μm size fraction (Tab. 2).

In the 10 m layer sample of station 80, large tabular gypsum crystals measuring up to 1 cm in length (mean length: 3,078 μm, mean width: 1,830 μm) dominated the >63 μm size fraction. Their average length-width ratio was 1.7. This size fraction contributed 89.1% of the gypsum mass (Figs. 5, S5, Tab. 2). The >30<63 μm size fraction was composed of fragments of these large crystals and few small gypsum needles. These often intergrown columnar crystals looked bladed, for most part also dented and with numerous cracks. Their mean length was 71.8 μm. The ice core retrieved from this station was very porous and broke into pieces of 9 to 11 cm. Cryogenic gypsum was retrieved from all these ice core sections and revealed a dominance of extraordinary large crystals (Figs. 5, S5), resembling the ROVnet samples from this station. The largest cryogenic gypsum crystals >6,000 μm (mean crystal length: 2,821 μm, mean width: 1,689 m) were retrieved from the top-most 8 cm ice core section, whereas, the maximum crystal size gradually decreased downcore (Fig. S5). The crystals themselves lacked sharp corners, and the large crystals had cavities inside, indicating an advanced stage of dissolution (Figs. 5C-D; S5).

Gelöscht: S3

Gelöscht: S4

Gelöscht: S4

Gelöscht: S4

Gelöscht: S4

3.3 Dissolution experiments

3.3.1 Experiments to simulate cryogenic gypsum dissolution within the Arctic water column

Our study area was characterized by the presence of three main water masses (Nikolopoulos et al., 2018; Rudels, 2015): 1) The Polar Surface Water (PSW) including the halocline, with a variable mean salinity of 32 and a temperature range of -1.8 to 0.0 °C, extended from the surface to maximum 100 m water depth (Nikolopoulos et al., 2018). 2) The Atlantic Water (AW) with a mean salinity of 34.4 to 34.7 and variable temperature of 0.0 to 4.7 °C in the study area extended from below the PSW to 600-800 m water depth (Nikolopoulos et al., 2018). 3) The Eurasian Arctic Deep Water (EADW) fills the deep Eurasian Basin below the AW with a temperature range of <0 to -0.94 °C and a salinity of about 34.9 (Nikolopoulos et al., 2018).

The dissolution experiments carried out to simulate dissolution in the PSW were set to 3 bar, -0.5 °C. Over the 24 hours lasting PSW-simulating dissolution experiment, about 6% of the gypsum dissolved (Figs. 6, S6A, Tab. 3). In the AW experiment, the combination of positive temperatures (2.5 °C) and a pressure of 65 bar impacted the dissolution on the cryogenic gypsum crystals more than in any other seawater trial. More than 80% of the cryogenic gypsum crystals dissolved during the 24-hours experiment (Figs. 6, S6B, Tab. 3). Moreover, as dissolution mainly affects the crystal's surface, smaller gypsums crystals and those with increased surface roughness were preferentially impacted by dissolution, whereas larger and solid crystals with smooth surface showed the lowest dissolution (Fig. S6B). The EADW-simulating dissolution experiments set to a temperature of -0.5 °C showed a progressive cryogenic gypsum dissolution of 26, 58, and 62% with increasing pressure for the 100, 120 and 150 bar experiments, respectively (Figs. 6, S7, Tab. 3).

Gelöscht: S5A

Gelöscht: S5B

Gelöscht: S5B

Gelöscht: S6

3.3.2 Experiments to simulate cryogenic gypsum dissolution within Formaldehyde-treated biological samples

In the Formaldehyde experiments we exposed our set of cryogenic gypsum crystals to a Formaldehyde solution of 4%, which is commonly used to store pelagic samples from the Polar Oceans (Edler, 1979). Irrespective of the temperature at which the sample was stored, all gypsum dissolved within 24 hours.

3.4 Sinking velocities of gypsum crystals

The sinking velocity (*SV*) of the gypsum crystals increased with crystal size (Fig. 7). Small crystals with an equivalent spherical diameter (*ESD*) of 200 μm sank with 300 m d^{-1} while large gypsum crystals with ESDs of 2,000 to 2,500 μm sank with velocities of 5,000 to 7,000 m d^{-1}. The size to settling relationship was best described by a power function ($SV = 4239.9\ ESD^{0.839}$, $R^2 = 0.84$).

Gelöscht: 7A

Gelöscht: As the power function suggests, the settling velocity levelled off for the largest gypsum crystals (Fig. 7A). The observed excess density of all crystals was smaller than is expected from the density of gypsum (2310 kg/m³). For the visually non porous smaller crystals drag, the deviation of gypsum crystals from round particles, and dissolution may be the main reason for the calculated lower density.¶ However, plotting the excess density as a function of size (Fig. 7B) also showed that the excess density of the gypsum decreased with increasing crystal size. The microscopic images show that large crystals were more porous and had more complex shapes (Fig. S8 A-C) compared to the small crystals that were more spherical and less porous (Figs. 2, 4-5, S8 D). Hence, the flat settling to size relationship for large gypsum crystals (Fig. 7A), was essentially due to a combination of increased porosity causing decreasing excess density and increased drag due to the complex shapes of the large crystals.

4 Discussion

4.1 Distribution and morphology of cryogenic gypsum crystals

This study shows for the first time the wide-spread presence of cryogenic gypsum under melting Arctic sea ice of different origin. At all stations cryogenic gypsum dominated the sample fraction of particles >30 μm in Eurasian Basin surface waters, indicating a continuous cryogenic gypsum flux from melting sea ice over a period of six weeks.

When designing the ROVnet for cryogenic gypsum sampling, we opted for the coarser >30 μm mesh to prohibit an overflow of the sampling container when running into a phytoplankton bloom. However, as Geilfus et al. (Geilfus et al., 2013) had observed gypsum crystals as small as 10 μm, we probably lost an unknown proportion of smaller gypsum crystals by the chosen sampling strategy. The gypsum crystals described from sea ice so far retrieved from only 3-days-old experimental and 30 cm thick natural sea ice off Greenland were small (crystal length max. 100 μm), planar euhedral gypsum crystals often intergrown or as rosettes (Geilfus et al., 2013). Similar, but larger (crystal length up to 1 mm), gypsum crystals were observed within *Phaeocystis* aggregates collected in the region of the present study (Wollenburg et al., 2018a). However, here we show that gypsum crystals exhibit a strong variability in size and morphology. Particularly large crystals were characterised by more complex shapes (Fig. 2, 5, S3-4) and increased surface roughness (Figs. S7C-D), compared to the small planar euhedral (Fig. 2A) and more spherical crystals (Fig. S7A-B). Euhedral crystal needles larger but otherwise similar to those described by Geilfus et al. (Geilfus et al., 2013) and Wollenburg et al. (Wollenburg et al., 2018a) dominated the >63 μm fraction collected at 5 and 10 m depths at station 66, and smaller crystals contributed especially to the >30<63 μm size fraction of the station's subsurface samples.

As cryogenic gypsum forms in sea ice brine pockets or channels, the size and morphology especially of large crystals is likely determined by sea ice texture and porosity during gypsum precipitation. Pursuing this hypothesis, the large and intergrown crystals collected from the 0 m layer at station 66, and the 10 m layer and ice-core at station 80, formed in highly branched granular sea ice (Lieb-Lappen et al., 2017; Weissenberger et al., 1992). In contrast, the small cryogenic gypsum needles reported by Geilfus et al. (Geilfus et al., 2013) and Wollenburg et al. (Wollenburg et al., 2018a), may have preferentially formed in columnar sea ice. Even sampling the same ice-floe (station 32 and 80), the appearance of the crystals changed. Possibly, a widening of the brine channels during the elapsed time (6 weeks) allowed a release of larger crystals at station 80 when compared to station 32. However, crystal growth during this elapsed period or lateral advection of large crystals cannot be excluded. Thus, detailed texture analyses on sea ice cores prior to sampling are needed to

Gelöscht: warming

Gelöscht: porosity

Gelöscht: S6A-C

Gelöscht: S6D

validate or reject hypotheses on a link between sea ice porosity and cryogenic gypsum crystal size and morphology and should be considered in future studies.

The sea ice microstructure dictating the formation of gypsum crystals in the brine matrix likely varied among ice-floes due to different ages, origins and drift trajectories (Fig. 1B). For example, station 66 was the only station where the sea ice likely formed over the central Nansen Basin only months before our study (Fig. 1B). The surface sample of station 66 had large intergrown hyaline star-shaped gypsum crystals that were observed at no other station. They also showed a considerably higher length-width ratio than crystals from second-year ice of stations 32/80 and 45 (Fig. 1B; Fig. 2). Accordingly, a close relationship between local sea ice properties and gypsum crystal morphology in the underlying water was evident from the comparison of gypsum crystals collected with the ROVnet with those retrieved from ice cores collected at two stations. The ice-core samples revealed cryogenic gypsum crystals that basically resembled the crystal morphologies collected from the water column at the same stations, indicating that the gypsum morphologies observed in the water column likely reflect the gypsum precipitation conditions and brine-channel structure of local ice-floes. The current understanding of mineral precipitation in supersaturated brines relies on ice-core analyses, sea ice brine- and experimental studies, and on mathematical modelling of the temperature window in which each mineral is likely to form (Butler et al., 2017; Marion et al., 2010). There are still many uncertainties regarding the precipitation and dissolution of gypsum within natural sea ice and during ice-core storage. Although the FREZCHEM model and Gitterman Pathway predict gypsum precipitation under defined conditions, only Geilfus et al. (Geilfus et al., 2013) and Butler et al. (Butler et al., 2017) succeeded in retrieving gypsum under such conditions, whereas others failed (Butler and Kennedy, 2015). According to the FREZCHEM model, cryogenic gypsum precipitates at temperatures of -6.2 to -8.5 °C and at temperatures <-18 °C (Geilfus et al., 2013; Wollenburg et al., 2018a). Accordingly, a storage temperature of -20 °C would allow the post-coring precipitation of gypsum from contained brines. However, in field and experimental studies cryogenic gypsum was so far only observed to precipitate in the -6.2 to -8.5 °C temperature window, even when treatments were conducted below -20 °C (Butler et al., 2017; Geilfus et al., 2013). Furthermore, the observed signs of dissolution on the large cryogenic gypsum crystals from the ice-core when compared to the sharp-edged crystals retrieved from the water column at station 80 indicate that significant new precipitation of gypsum during storage did not occur, rather the opposite.

Gelöscht: these

Apart from the growing conditions of gypsum crystals within sea ice, the size spectrum of crystals retrieved from different depths in the water column likely was essentially altered by the size-dependent sinking velocity of the crystals. Because the sinking velocity of large cryogenic gypsum crystals is high the chance to catch large crystals with horizontal transects directly under the ice should be lower compared to small crystals (Fig. 7A). Accordingly, significant amounts of large cryogenic gypsum crystals were mainly sampled from the 0 m layer where they could be scraped off the underside of the ice (see station 66, Tab. 2). In contrast, smaller cryogenic gypsum crystals sink at lower velocities (Fig. 7A). Hence, the large quantity of small-sized crystals retrieved in the deeper layers of station 66, and all layers of station 32 and 45 likely were influenced by the accumulated gypsum release in this size-fraction, whereas the rarer large crystals indicated the momentary release at these stations. The extremely large crystals sampled at station 80 at 10 m depth probably indicated an on-going flux event during rapid melting. According to our dissolution experiments, gypsum dissolution within Arctic surface waters should only have a minor impact on the size distribution of cryogenic gypsum crystals within the surface water. Besides vertical flux, advection of gypsum crystals with surface currents may also have influenced the size-distribution of gypsum crystals sampled in the water column.

4.2 Reasons why cryogenic gypsum was rarely observed in past studies

The small temperature range of the -6.2 to -8.5 °C window, which is also the only gypsum precipitation temperature spectrum applicable in the Arctic Ocean, has been considered one reason why gypsum was not detected in other studies (Butler and Kennedy, 2015; Wollenburg et al., 2018a). Furthermore, the kinetics of gypsum precipitation was considered as too slow for detection during experimental studies, and the amount of gypsum hard to verify versus other sea ice precipitates that are quantitatively much more abundant, leading the focus towards other sea ice precipitates (Butler and Kennedy, 2015; Geilfus et al., 2013). Although cryogenic mirabilite and hydrohalite are three and twenty-two times more abundant than gypsum, respectively (Butler and Kennedy, 2015), gypsum is the only sea ice precipitate that survives for one to several days within the Arctic water column. Cryogenic gypsum dissolution increases with increasing hydrostatic pressure and increasing temperatures (Fig. 6). However, well-preserved cryogenic gypsum crystals were retrieved from algae aggregates collected from 2,146 m water depth, suggesting that either the transport from the surface to

Gelöscht:

this depth was very rapid or that dissolution was decreased and/or prevented once gypsum crystals were included within the matrix of organosulfur compound-rich aggregates (Wollenburg et al., 2018a). Yet, as seawater is usually undersaturated with respect to gypsum (Briskin and Schreiber, 1978a; Briskin and Schreiber, 1978b) and is shown by our dissolution experiments, disaggregation of organic aggregates would expose the gypsum to the seawater and dissolve any crystals making it to the deep ocean or seafloor likely within a few days. The same dissolution would occur within the sampling cups of sediment traps, explaining why gypsum has not been observed in those type of samples.

Our dissolution experiments showed that cryogenic gypsum can persist long enough in the cold polar surface water to be collected in measurable concentrations. The missing evidence of gypsum from past studies was likely due to the quick dissolution of gypsum crystals at higher temperatures and pressure dependence of dissolution kinetics, impeding the discovery of gypsum in sediment trap samples and on the sea-floor. In addition, Formaldehyde preservation leads to the immediate dissolution of gypsum, destroying any evidence of cryogenic gypsum in all kinds of biological samples including water column and net samples. Based on our experience with the PS106 expedition samples and the experiments presented here, we propose a standardized procedure for gypsum sampling in the field. This procedure is part of the standard operating protocol for gypsum samplind on the MOSAIC expedition (S 9).

Gelöscht: too,

4.3 Potential of cryogenic gypsum as a ballast of algae blooms

We found less than 6% dissolution of individual crystals in Polar Surface Water (PSW) per day. Thus, at depths immediately below the fluorescence maximum where a significant part of organic aggregates are formed (Iversen et al. 2010), the gypsum scavenging and ballasting of aggregates (Turner, 2015) is little affected by gypsum dissolution (Olli et al., 2007) (Fig. 6, Tab. 3). Incorporation of dense minerals into settling organic aggregates will increase their density and, therefore, the size-specific sinking velocities of the aggregates (Iversen and Ploug, 2010; Iversen and Robert, 2015; van der Jagt et al., 2018). The high sinking velocity of large gypsum crystals >1 mm (5,000-7,000 m d^{-1} (Fig. 7A)) could create strong hydrodynamic shear that might cause disaggregation of fragile algae aggregates (Olli et al., 2007). However, smaller gypsum crystals have been observed inside *Phaeocystis* aggregates collected at depths below 2000 m (Wollenburg et al. 2018a). This shows that cryogenic gypsum is incorporated

into organic aggregates and supports that gypsum can be an important ballast mineral of organic aggregates.

As chlorophyll concentrations in the surface water were mostly low (< 1 mg m^{-3}, H.F. unpublished data), a massive gypsum-mediated export of phytoplankton was unlikely during expedition PS106. However, especially at the ice floe of station 32/80, we observed a high coverage of the ice underside by the filamentous algae *Melosira arctica*, and gypsum crystals were found in *M. arctica* filaments collected nearby (Fig. 8) as well as at station 45 (Fig. 2D). This indicates a potential for rapid *M. arctica* downfall mediated by cryogenic gypsum, as soon as the algal filaments were released from the melting sea ice. Hence, ballasting by cryogenic gypsum may also have contributed to the mass export of *Melosira arctica* aggregates observed in 2012 (Boetius et al. 2013).

Gelöscht: This
Gelöscht: previous suggestions of
Gelöscht: as
Gelöscht: , such as *Phaeocystis* (Wollenburg et al., 2018a) by rather small crystals
Gelöscht: Figs.
Gelöscht: , 8
Formatiert: Schriftart: (Standard) Times, Englisch (Vereinigtes Königreich)

5 Conclusions

This study shows for the first time that gypsum released to the water at the onset of melt season in the Arctic Ocean causes a constant flux of gypsum over wide spread areas and over a long period of time (> six weeks). The morphological diversity of gypsum crystals retrieved from Arctic surface waters and ice-cores indicated a complex variety of precipitation and release processes as well as modifications during sea ice formation, the melt phase, and in the water column. In the fresh and cold Polar surface water, gypsum crystals persist long enough to act as an effective ballast on organic matter, such as phytoplankton filaments and marine snow.

References:

Arrigo, K. R., Perovich, D. K., Pickart, R. S., Brown, Z. W., van Dijken, G. L., Lowry, K. E., Mills, M. M., Palmer, M. A., Balch, W. M., Bahr, F., Bates, N. R., Benitez-Nelson, C., Bowler, B., Brownlee, E., Ehn, J. K., Frey, K. E., Garley, R., Laney, S. R., Lubelczyk, L., Mathis, J., Matsuoka, A., Mitchell, B. G., Moore, G. W. K., Ortega-Retuerta, E., Pal, S., Polashenski, C. M., Reynolds, R. A., Schieber, B., Sosik, H. M., Stephens, M., and Swift, J. H.: Massive Phytoplankton Blooms Under Arctic Sea Ice, Science, 336, 1408, 2012.

Arrigo, K. R., Perovich, D. K., Pickart, R. S., Brown, Z. W., van Dijken, G. L., Lowry, K. E., Mills, M. M., Palmer, M. A., Balch, W. M., Bates, N. R., Benitez-Nelson, C. R., Brownlee, E., Frey, K. E., Laney, S. R., Mathis, J., Matsuoka, A., Greg Mitchell, B., Moore, G. W. K., Reynolds, R. A., Sosik, H. M., and Swift, J. H.: Phytoplankton blooms beneath the sea ice in the Chukchi sea, Deep Sea Research Part II: Topical Studies in Oceanography, 105, 1-16, 2014.

Assmy, P., Fernández-Méndez, M., Duarte, P., Meyer, A., Randelhoff, A., Mundy, C. J., Olsen, L. M., Kauko, H. M., Bailey, A., Chierici, M., Cohen, L., Doulgeris, A. P., Ehn, J. K., Fransson, A., Gerland, S., Hop, H., Hudson, S. R., Hughes, N., Itkin, P., Johnsen, G., King, J. A., Koch, B. P., Koenig, Z., Kwasniewski, S., Laney, S. R., Nicolaus, M., Pavlov, A. K., Polashenski, C. M., Provost, C., Rösel, A., Sandbu, M., Spreen, G., Smedsrud, L. H., Sundfjord, A., Taskjelle, T., Tatarek, A., Wiktor, J., Wagner, P. M., Wold, A., Steen, H., and Granskog, M. A.: Leads in Arctic pack ice enable early phytoplankton blooms below snow-covered sea ice, Scientific Reports, 7, 40850, 2017.

Briskin, M. and Schreiber, B. C.: Authigenic gypsum in marine sediments, Marine Geology, 28, 37-49, 1978.

Butler, B.: Mineral dynamics in sea ice brines, PhD, Bangor, 184 pp., 2016.

Butler, B. M. and Kennedy, H.: An investigation of mineral dynamics in frozen seawater brines by direct measurement with synchrotron X-ray powder diffraction, Journal of Geophysical Research: Oceans, 120, 5686-5697, 2015.

Butler, B. M., Papadimitriou, S., Day, S. J., and Kennedy, H.: Gypsum and hydrohalite dynamics in sea ice brines, Geochimica et Cosmochimica Acta, 213, 17-34, 2017.

Culberson, C. and Pytkowicx, R. M.: Effect of pressure on carbonic acid, boric acid, and the pH in seawater, Limnology and Oceanography, 13, 403-417, 1968.

Damm, E., Bauch, D., Krumpen, T., Rabe, B., Korhonen, M., Vinogradova, E., and Uhlig, C.: The Transpolar Drift conveys methane from the Siberian Shelf to the central Arctic Ocean, Scientific Reports, 8, 4515, 2018.

Docquier, D., Massonnet, F., Barthélemy, A., Tandon, N. F., Lecomte, O., and Fichefet, T.: Relationships between Arctic sea ice drift and strength modelled by NEMO-LIM3.6, The Cryosphere, 11, 2829-2846, 2017.

Edler, L.: Recommendations on Methods for Marine Biological Studies in the Baltic Sea: Phytoplankton and chlorophyll, Department of Marine Botany, University of Lund, 1979.

Flores, H. E., J.; Lange, B.; Sulanke, E.; Niehoff, B.; Hildebrandt, N.; Doble, M.; Schaafsma, F.; Meijboom, A.; Fey, B.; Kühn, S.; Bravo-Rebolledo; E.; Dorssen, M. van; Grandinger, R.; Hasset, B.; Kunisch, E.; Kohlbach, D.; Graeve, M.; Franeker, J. A. van; Gradinger, Bluhm, B.: Under-ice fauna, zooplankton and endotherms. In: The Expeditions PS106/1 and 2 of the Research Vessel Polarstern to the Arctic Ocean in 2017, Macke, A. F., H. (Ed.), Reports on polar and marine research, 2018.

Geilfus, N. X., Galley, R. J., Cooper, M., Halden, N., Hare, A., Wang, F., Søgaard, D. H., and Rysgaard, S.: Gypsum crystals observed in experimental and natural sea ice, Geophysical Research Letters, 40, 6362-6367, 2013.

Girard-Ardhuin, F. and Ezraty, R.: Enhanced Arctic Sea Ice Drift Estimation Merging Radiometer and Scatterometer Data, IEEE Transactions on Geoscience and Remote Sensing, 50, 2639-2648, 2012.

Golden, K. M., Ackley, S. F., and Lytle, V. I.: The Percolation Phase Transition in Sea Ice, Science, 282, 2238, 1998.

Iversen, M., Nowald, N., Ploug, H., A. Jackson, G., and Fischer, G.: High resolution profiles of vertical particulate organic matter export off Cape Blanc, Mauritania: Degradation processes and ballasting effects, Deep Sea Research Part I Oceanographic Research Papers, 57, 771-784, 2010.

Iversen, M. H. and Ploug, H.: Ballast minerals and the sinking carbon flux in the ocean: carbon-specific respiration rates and sinking velocity of marine snow aggregates, Biogeosciences, 7, 2613-2624, 2010.

Iversen, M. H. and Robert, M. L.: Ballasting effects of smectite on aggregate formation and export from a natural plankton community, Marine Chemistry, 175, 18-27, 2015.

Katlein, C., Arndt, S., Nicolaus, M., Perovich, D. K., Jakuba, M. V., Suman, S., Elliott, S., Whitcomb, L. L., McFarland, C. J., Gerdes, R., Boetius, A., and German, C. R.: Influence of ice thickness and surface properties on light transmission through Arctic sea ice, Journal of Geophysical Research: Oceans, 120, 5932-5944, 2015.

Katlein, C., Nicolaus, M., Sommerfeld, A., Copalorado, V., Tiemann, L., Zanatta, M., Schulz, H., and Lange, B.: Sea Ice Physics. In: The Expeditions PS106/1 and 2 of the research vessel Polarstern in the Arctic Ocean in 2017, Macke, A. F., H. (Ed.), Berichte zur Polarforschung Bremerhaven, 2018.

Katlein, C., Schiller, M., Belter, H. J., Coppolaro, V., Wenslandt, D., and Nicolaus, M.: A New Remotely Operated Sensor Platform for Interdisciplinary Observations under Sea Ice, Frontiers in Marine Science, 4, 281, 2017.

Krumpen, T.: AWI ICETrack - Antarctic and Arctic Sea Ice Monitoring and Tracking Tool Alfred-Wegener-Institut Hemholtz-Zentrum für Polar- und Meeresforschung, Bremerhaven, Germany, 2018.

Krumpen, T., Belter, H. J., Boetius, A., Damm, E., Haas, C., Hendricks, S., Nicolaus, M., Nöthig, E.-M., Paul, S., Peeken, I., Ricker, R., and Stein, R.: Arctic warming interrupts the Transpolar Drift and affects long-range transport of sea ice and ice-rafted matter, Scientific Reports, 9, 5459, 2019.

Krumpen, T., Gerdes, R., Haas, C., Hendricks, S., Herber, A., Selyuzhenok, V., Smedsrud, L., and Spreen, G.: Recent summer sea ice thickness surveys in Fram Strait and associated ice volume fluxes, The Cryosphere, 10, 523-534, 2016.

Kwok, R.: Arctic sea ice thickness, volume, and multiyear ice coverage: losses and coupled variability (1958–2018), Environmental Research Letters, 13, 105005, 2018.

Kwok, R. and Rothrock, D. A.: Decline in Arctic sea ice thickness from submarine and ICESat records: 1958-2008, Geophys. Res. Lett., 36, 2009.

Lavergne, T.: Validation and Monitoring of the OSI SAF Low Resolution Sea Ice Drift Product (v5), 2016.

Lieb-Lappen, R. M., Golden, E. J., and Obbard, R. W.: Metrics for interpreting the microstructure of sea ice using X-ray micro-computed tomography, Cold Regions Science and Technology, 138, 24-35, 2017.

Marion, G. M., Mironenko, M. V., and Roberts, M. W.: FREZCHEM: A geochemical model for cold aqueous solutions, Computers & Geosciences, 36, 10-15, 2010.

Nicolaus, M., Arndt, S., Katlein, C., Maslanik, J., and Hendricks, S.: Correction to “Changes in Arctic sea ice result in increasing light transmittance and absorption”, Geophysical Research Letters, 40, 2699-2700, 2013.

Nicolaus, M., Katlein, C., Maslanik, J., and Hendricks, S.: Changes in Arctic sea ice result in increasing light transmittance and absorption, Geophysical Research Letters, 39, 2012.

Nikolopoulos, A., Heuzé, C., Linders, T., Andrée, E., and Sahlin, S.: Physical Oceanography. In: The Expeditions PS106/1 and 2 of the Research Vessel POLARSTERN to the Arctic Ocean in 2017, Macke, A. and Flores, H. (Eds.), Reports on Polar and Marine Research, Alfred-Wegener Institute Helmholtz Centre for Polar and marine research, Bremerhaven, 2018.

Nürnberg, D., Wollenburg, I., Dethleff, D., Eicken, H., Kassens, H., Letzig, T., Reimnitz, E., and Thiede, J.: Sediments in Arctic sea ice: Implications for entrainment, transport and release, Marine Geology, 119, 185-214, 1994.

Olli, K., Wassmann, P., Reigstad, M., Ratkova, T. N., Arashkevich, E., Pasternak, A., Matrai, P. A., Knulst, J., Tranvik, L., Klais, R., and Jacobsen, A.: The fate of production in the central Arctic Ocean - top-down regulation by zooplankton expatriates?, Progress In Oceanography, 72, 84-113, 2007.

Peeken, I., Primpke, S., Beyer, B., Gütermann, J., Katlein, C., Krumpen, T., Bergmann, M., Hehemann, L., and Gerdts, G.: Arctic sea ice is an important temporal sink and means of transport for microplastic, Nature Communications, 9, 1505, 2018.

Peeken, I. C., G.; Flores, H.; Ehrlich, J.; Lange, B.; Schaafsma, F., Gradinger, R.; Hassett, B.; Kunisch, E.; Damm, E.; Verdugo, J.; Kohlbach, D.; Graeve, M.; Bluhm, B.: Sea ice biology and biogeochemistry. In: The Expeditions PS106/1 and 2 of the Research Vessel Polarstern to the Arctic Ocean in 2017, Macke, A. F., H. (Ed.), 719, Reports of polar and marine research, 2018.

Ploug, H., Iversen, M. H., Koski, M., and Buitenhuis, E. T.: Production, oxygen respiration rates, and sinking velocity of copepod fecal pellets: Direct measurements of ballasting by opal and calcite, Limnology and Oceanography, 53, 469-476, 2008.

764 Rudels, B.: Arctic Ocean circulation, processes and water masses: A description of
765 observations and ideas with focus on the period prior to the International Polar Year 2007–
766 2009, Progress in Oceanography, 132, 22-67, 2015.
767
768 Schneider, C. A., Rasband, W. S., and Eliceiri, K. W.: NIH Image to ImageJ: 25 years of image
769 analysis, Nature Methods, 9, 671, 2012.
770
771 Smedsrud, L. H., Halvorsen, M. H., Stroeve, J. C., Zhang, R., and Kloster, K.: Fram Strait sea ice
772 export variability and September Arctic sea ice extent over the last 80 years, The Cryosphere,
773 11, 65-79, 2017.
774
775 Strunz, H. and Nickel, E. H.: Strunz Mineralogical Tables. Chemical-structural Mineral
776 Classification System, Schweizerbart'sche Verlagsbuchhandlung (Nägele u. Obermiller),
777 Stuttgart, 2001.
778
779 Tschudi, S., Fowler, C., Maslanik, J., Stewart, J., and Stewart, W.: Polar Pathfinder Daily 25 km
780 EASE-Grid Sea Ice Motion Vectors. In: Technical report, NASA National Snow and Ice Data
781 Center Distributed Active Archive Center, Boulder, Colorado USA 2016.
782
783 Turner, J. T.: Zooplankton fecal pellets, marine snow, phytodetritus and the ocean's
784 biological pump, Progress in Oceanography, 130, 205-248, 2015.
785
786 van der Jagt, H., Friese, C., Stuut, J.-B. W., Fischer, G., and Iversen, M. H.: The ballasting
787 effect of Saharan dust deposition on aggregate dynamics and carbon export: Aggregation,
788 settling, and scavenging potential of marine snow, Limnology and Oceanography, 63, 1386-
789 1394, 2018.
790
791 Vogel, S. and Beety, S. T.: Life in Moving Fluids: The Physical Biology of Flow, Princeton
792 University Press, 1994.
793
794 Weissenberger, J., Dieckmann, G., Gradinger, R., and Spindler, M.: Sea ice: A cast technique
795 to examine and analyze brine pockets and channel structure, Limnology and Oceanography,
796 37, 179-183, 1992.
797
798 White, F. M.: Viscous fluid flow, McGraw-Hill, 1974. 614, 1974.
799
800 Wollenburg, J. E., Katlein, C., Nehrke, G., Nöthig, E. M., Matthiessen, J., Wolf- Gladrow, D. A.,
801 Nikolopoulos, A., Gázquez-Sanchez, F., Rossmann, L., Assmy, P., Babin, M., Bruyant, F.,
802 Beaulieu, M., Dybwad, C., and Peeken, I.: Ballasting by cryogenic gypsum enhances carbon
803 export in a Phaeocystis under-ice bloom, Scientific Reports, 8, 7703, 2018a.
804
805 Wollenburg, J. E., Zittier, Z. M. C., and Bijma, J.: Insight into deep-sea life – Cibicidoides
806 pachyderma substrate and pH-dependent behaviour following disturbance, Deep Sea
807 Research Part I: Oceanographic Research Papers, 138, 34-45, 2018b.
808
809
810

Table captions:

Tab. 1: Properties of sea ice stations and characteristics of ROVnet profiles.

Cruise Site	Date	Latitude (Deg N)	Longitude (Deg E)	Ocean depth (m)	Sampling depth	Water temp. (°C)	Salinity	Mean ice thickness (m)	Filtered water volume (m^3)
PS106.1 Stat. 32	2017-06-15	81.73	10.86	1608	under-ice	-1.94	34.27	1.90	2.2
					5 m	n.a	n.a.	1.90	3.9
PS106.2 Stat. 45	2017-06-25	78.10	30.47	233	under-ice	-1.52	33.84	1.00	2.3
					5 m	-1.47	34.11	1.00	4.5
					10 m	-1.68	34.29	1.00	2.5
PS106.2 Stat. 66	2017-07-02	81.66	32.34	1506	under-ice	-1.67	33.18	1.80	3.1
					5 m	-1.71	33.76	1.80	2.7
					10 m	-1.73	33.78	1.80	3.1
PS106.2 Stat. 80	2017-07-12	81.37	17.13	1010	10 m	-1.37	32.87	1.80	1.7

Formatiert: Schriftart: Nicht Fett

[1] verschoben (Einfügung)

Formatiert: Links

Formatierte Tabelle

Formatiert: Hochgestellt

[1] nach oben verschoben: Tab. 1: Properties of sea ice stations and characteristics of ROVnet profiles.¶

Tab. 2: Size measurements and percentage of mass contribution of gypsum crystals from the >63 μm size fraction and the >30 < 63 μm size fraction

	>63 µm fraction			>30<63 µm fraction				
Cruise, Site, mean water depth of the catch	Mean length µm	Mean width µm	length/ width ratio	Mean length µm	Mean width µm	length/ width ratio	>63 µm fraction weight%	>30<63 µm fraction weight%
PS106.1, Stat. 32, 0 m	68.46	44.27	1.55	50.64	35.03	1.45	43.70	56.30
PS106.1, Stat. 32, 5 m	63.28	35.90	1.76	49.91	35.57	1.40	33.72	66.28
PS106.1, Stat. 32, mean (0-5 m)	65.87	40.09	1.64	50.28	35.30	1.42	38.71	61.29
PS106.2, Stat. 45, 0 m	114.18	65.93	1.73	58.74	42.84	1.37	79.90	20.10
PS106.2, Stat. 45, 5 m	110.98	64.84	1.71	56.73	38.89	1.46	73.39	26.61
PS106.2, Stat. 45 , 10 m	92.83	46.81	1.98	50.32	29.98	1.68	66.14	33.86
PS106.2, Stat. 45, mean (0-10 m)	85.49	44.45	1.92	77.93	24.28	3.21	73.14	26.86
PS106.2, Stat. 66, 0 m	1355.38	415.10	3.27	56.67	25.63	2.21	99.25	0.75
PS106.2, Stat. 66, 5 m	411.42	73.45	5.60	62.03	12.20	5.08	75.23	24.77
PS106.2, Stat. 66, 10 m	101.40	23.19	4.37	30.71	5.79	5.30	61.18	38.82
PS106.2, Stat. 66, mean (0-10 m)	599.17	164.78	3.64	59.96	12.61	4.76	58.16	41.84
PS106.2, Stat. 80, 10 m	3078.44	1830.00	1.68	71.78	30.76	2.33	89.05	10.95

Gelöscht:

	>63 µm fraction	
Cruise, Site, mean water depth of the catch	Mean length µm	Mean width µm
PS106.1, Stat. 32, 0 m	68.46	44.27
PS106.1, Stat. 32, 5 m	63.28	35.90
PS106.1, Stat. 32, mean (0-5 m)	65.87	40.09
PS106.2, Stat. 45, 0 m	114.18	65.93
PS106.2, Stat. 45, 5 m	110.98	64.84
PS106.2, Stat. 45 , 10 m	92.83	46.81
PS106.2, Stat. 45, mean (0-10 m)	85.49	44.45
PS106.2, Stat. 66, 0 m	1355.38	415.10
PS106.2, Stat. 66, 5 m	411.42	73.45
PS106.2, Stat. 66, 10 m	101.40	23.19
PS106.2, Stat. 66, mean (0-10 m)	599.17	164.78
PS106.2, Stat. 80, 10 m	3078.44	1830.00

Gelöscht: ¶ ... [1]

Formatiert: Abstand Nach: 10 Pt., Zeilenabstand: Mehrere 1.15 ze

Tab. 3: Dissolution experiments on cryogenic gypsum crystals. 'Water mass' simulating experiments with 34.9‰ sterile filtered seawater. Each experiment was conducted in parallel in 3-4 separate pressure chambers.

	Dissolution in weight%				
Chamber (no.)/Water mass	PSW	AW	EADW (1)	EADW (2)	EADW (3)
1	11.34	76.22	47.52	57.08	74.92
2	1.33	86.23	26.09	71.03	53.77
3	8.29	82.93	21.05	47.15	57.43
4	2.99	78.57	10.91	58.56	
Mean	**5.99**	**80.77**	**26.39**	**58.34**	**62.04**

Formatiert: Schriftart: 12 Pt.

Formatiert: Schriftart: Nicht Fett

831 **Figure captions:**

832

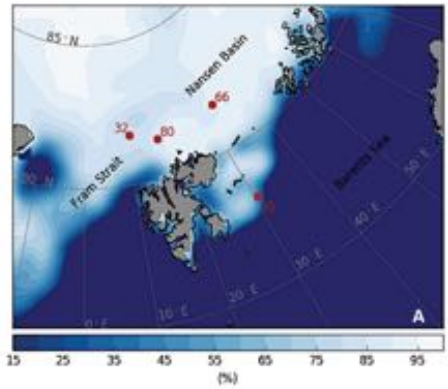
85 °N
Nansen Basin
66
32
80
Fram Strait
Barents Sea
A
15
25
35
45
55
65
75
85
95
(%)

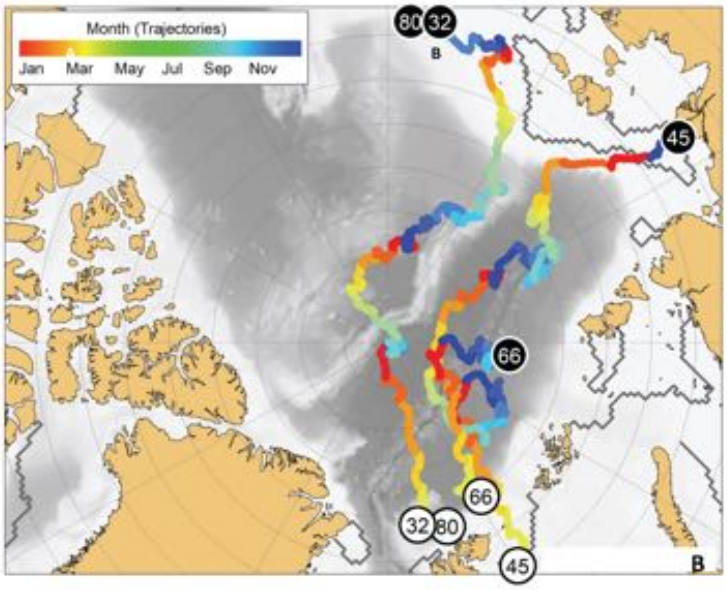
Month (Trajectories)
Jan
Mar
May
Jul
Sep
Nov
80
32
B
45
66
66
32
80
45
B

833

Gelöscht: Seitenumbruch

¶

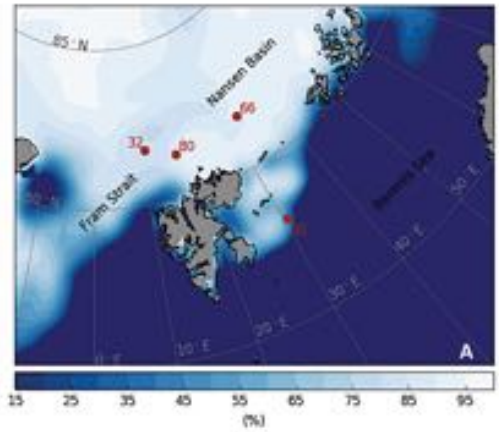

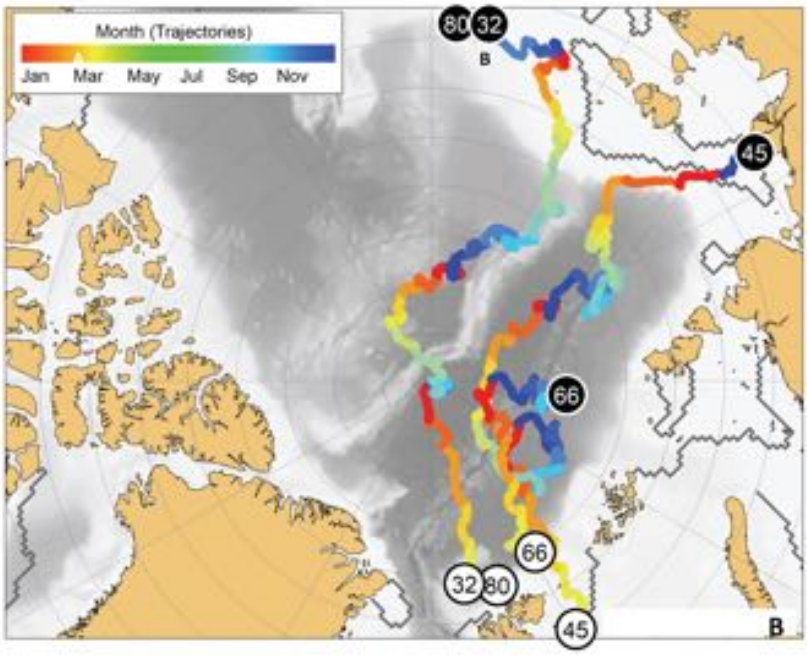

Fig. 1: Study area with sample locations. A: Sea ice coverage at the station and time of sampling in %. B) Trajectories of the sea ice from which the cryogenic gypsum was released. Each trajectory starts where sea ice formed (black circles), and shows its drift until the time

and place of sampling (white circles). The colour scale of the drift trajectories indicates the month in which the back-tracked sea ice was at any given position.

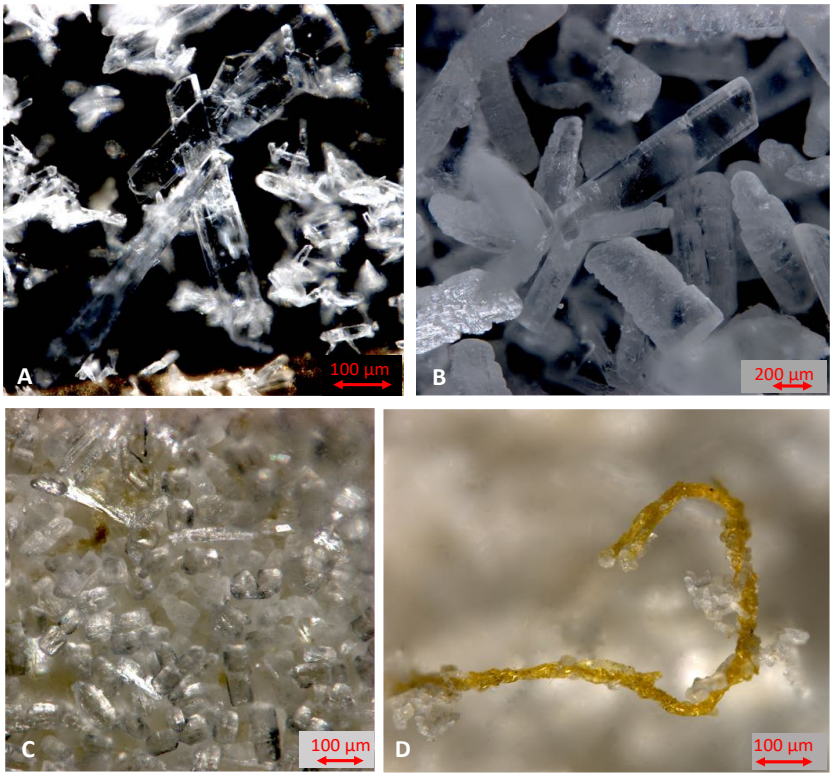

Fig. 2: Cryogenic gypsum crystals collected during Polarstern expedition PS106-1 from the upper water column. A) Crystals collected from station 66 at 5 m water depth. B) Crystals collected from station 66 at 0 m water depths. C) Crystals collected from station 45 at 10 m water depth. D) Crystals collected from station 45 at 10 m water depths entangled in an algae filament.

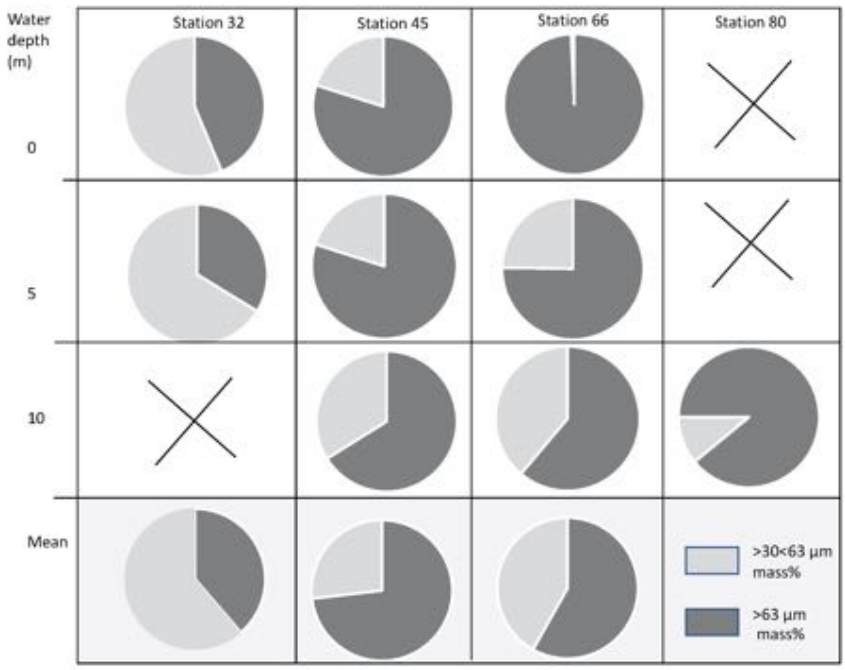

Fig. 3: Proportional mass (%) of cryogenic gypsum for the size fractions >30<63 μm and >63 μm for all ROV samples.

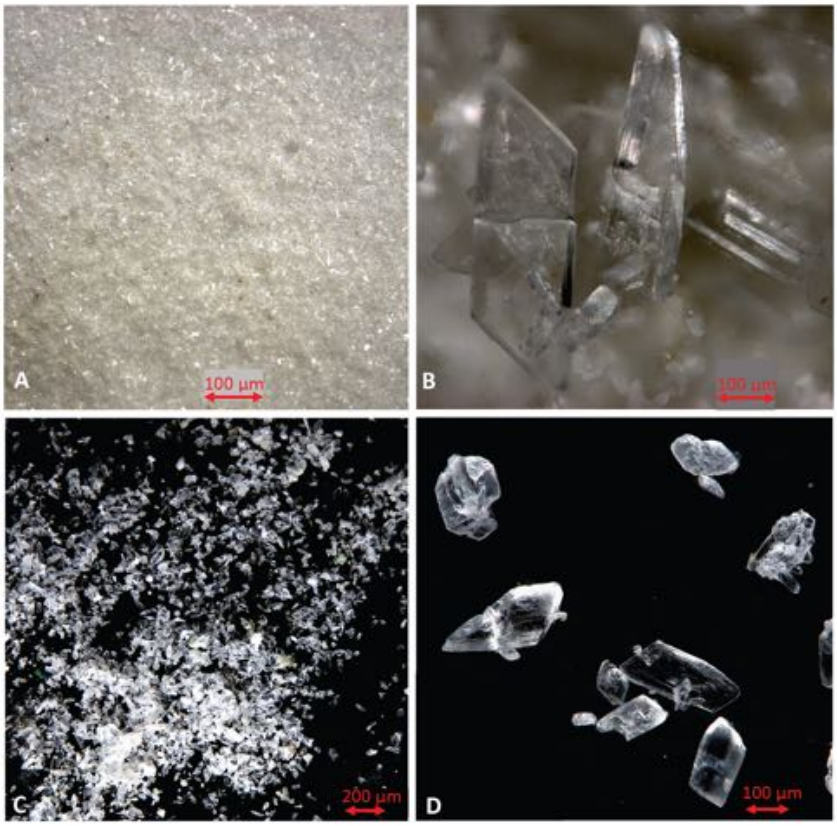

855

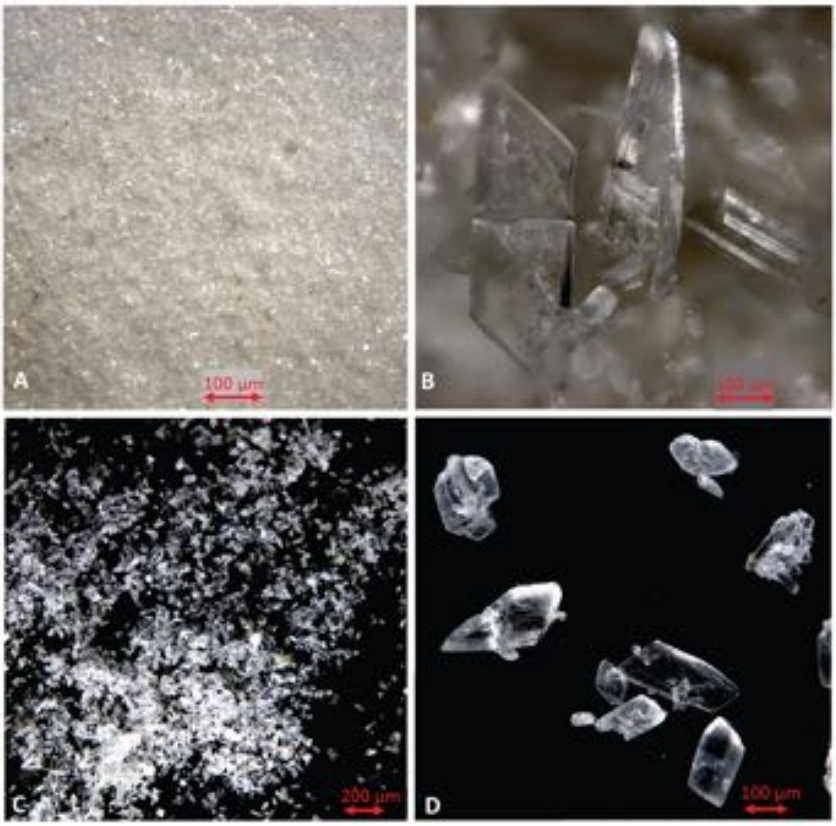

Fig. 4: Comparison of cryogenic gypsum crystals collected from the water column at station PS45 (10 m water depth) (A-B) with crystals retrieved from an ice-core collected above the ROVnet sampling area (C-D).

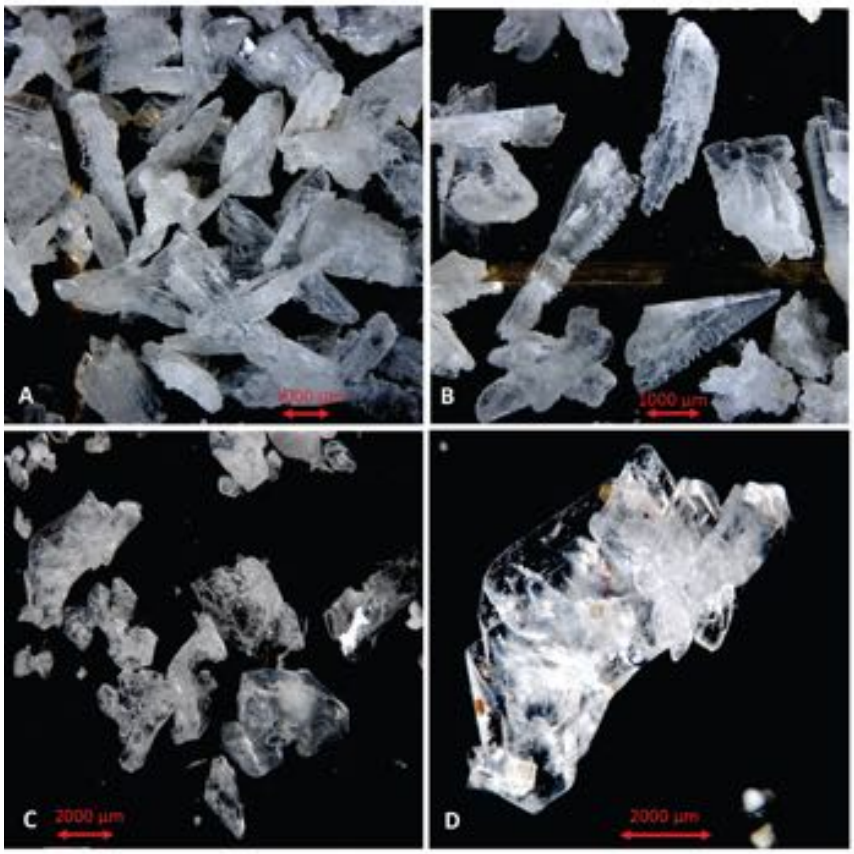

Fig. 5: Comparison of cryogenic gypsum crystals collected from the water column at station PS80-2 (10 m water depth) (A-B) with crystals retrieved from an ice-core collected above the ROVnet sampling area (C-D).

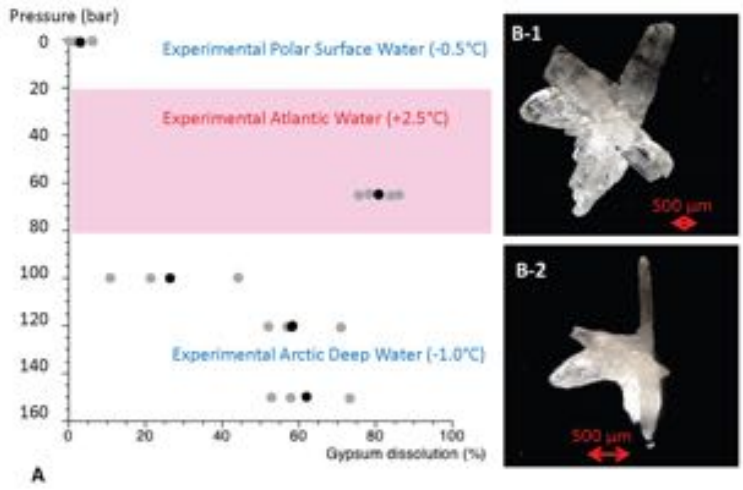

Figure 6: Results from cryogenic gypsum dissolution experiments. A) Graph showing the position of the simulated Arctic water masses in respect to pressure and temperature and how much gypsum (%) was dissolved on average over a 24-hours lasting exposure to such pressure and temperature conditions. Grey dots indicate the values from each aquarium, black dots the mean per experiment. B-1) Cryogenic gypsum crystal of the 120 bar-experiment before exposure. B-2) The same cryogenic gypsum crystal of the 120 bar-experiment after 24 hours.

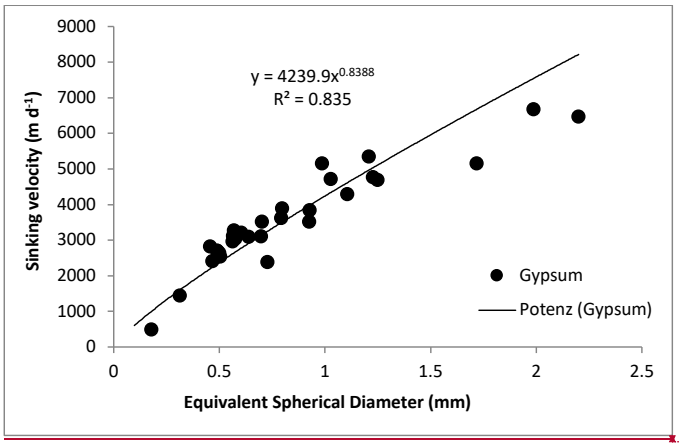

Fig. 7: sinking velocity of cryogenic gypsum crystals plotted against equivalent spherical diameter (ESD).

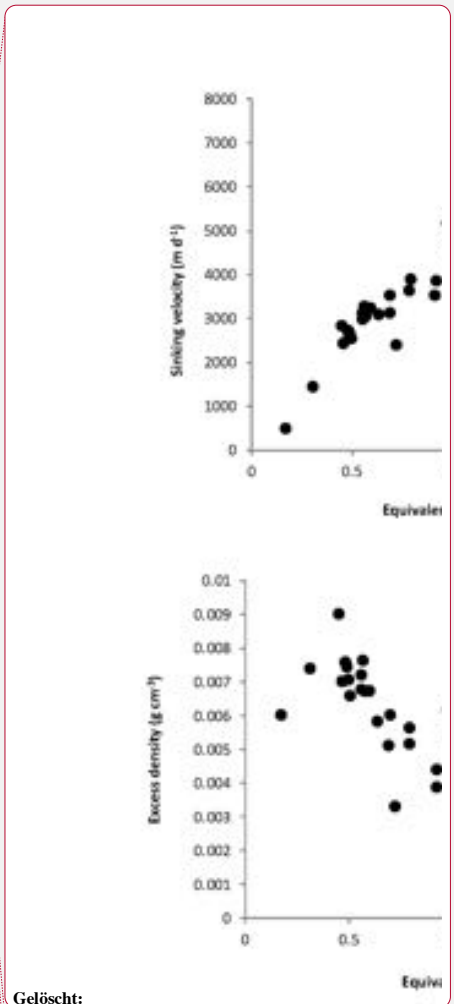

Gelöscht:

Formatiert: Deutsch

Gelöscht: (A)

Gelöscht: and (B) excess density (excess density = gypsum density – seawater density)

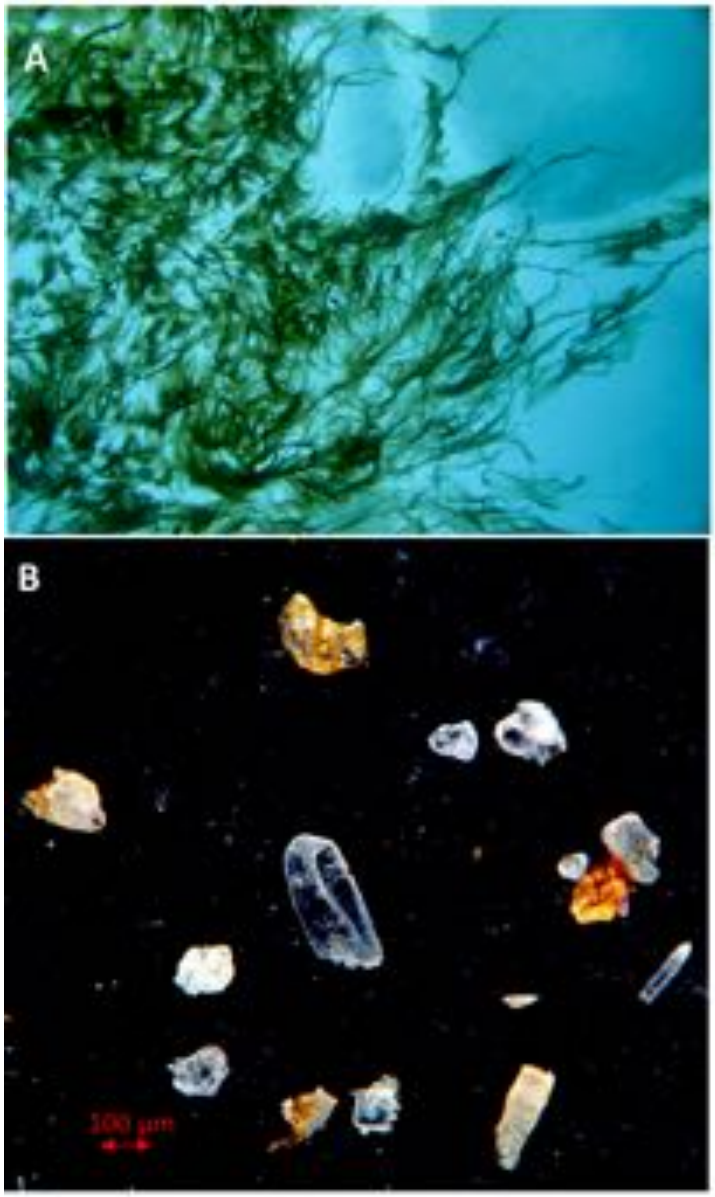

Fig. 8: Living *Melosira arctica* curtains hanging from ice flows during the PS106 expedition (photo taken by M. Nicolaus and C. Katlein). Cryogenic gypsum isolated from *Melosira arctica* (PS106-1, station 21(Peeken, 2018)).

Acknowledgement:

We thank Gernot Nehrke for performing Raman Spectroscopy on crystals from all catches. Christoph Vogt and Dieter Wolf-Gladrow made valuable comments on the manuscript. We thank the captain and crew of RV Polarstern expedition PS106 for their support at sea. This study was funded by the PACES (Polar Regions and Coasts in a Changing Earth System) Program of the Helmholtz Association, the Helmholtz Infrastructure Fund "Frontiers in Arctic Marine Monitoring (FRAM)". This study used samples and data provided by the Alfred-Wegener-Institut Helmholtz-Zentrum für Polar- und Meeresforschung in Bremerhaven from *Polarstern* expedition PS 106 (Grant No. AWI-PS106_00).

Author Contributions:

J.W., H.F: and M.I. designed this study. J.W. lead the writing of this manuscript and performed gypsum sample preparation and analysis. H.F., I.P., C.K., G.C., M.N. acquired ROVnet and ice samples in the field. M.I. measured crystal settling velocities. T.K. performed the backtracking analysis. All authors contributed to the writing and editing of the manuscript.

Gelöscht: and we thank them very much for it.

Formatiert: Zeilenabstand: 1.5 Zeilen

Gelöscht: as well as

Gelöscht: ¶

Seite 24: [1] Gelöscht **Wollenburg** **19.03.20 11:03:00**